*Human Molecular Genetics, 2014, Vol. 23, No. 19* **5147–5158**
*doi:10.1093/hmg/ddu238*
*Advance Access published on May 15, 2014*

# TUBB5 and its disease-associated mutations influence the terminal differentiation and dendritic spine densities of cerebral cortical neurons

**Linh Ngo[1,†], Matilda Haas[1,†], Zhengdong Qu[1], Shan Shan Li[1], Jennifer Zenker[1], Kathleen Sue Lyn Teng[3], Jenny Margaret Gunnersen[3,4], Martin Breuss[2], Mark Habgood[3], David Anthony Keays[2,*] and Julian Ik-Tsen Heng[1,*]**

[1]EMBL Australia, The Australian Regenerative Medicine Institute, Monash University, Clayton, VIC 3800, Australia, [2]Institute of Molecular Pathology, Dr Bohr-Gasse, Vienna 1030, Austria, [3]The Anatomy and Neuroscience Department, University of Melbourne, Parkville, VIC 3010, Australia and [4]The Florey Institute of Neuroscience and Mental Health, Parkville, VIC 3010, Australia

Received December 17, 2013; Revised April 16, 2014; Accepted May 12, 2014

**The microtubule cytoskeleton is critical for the generation and maturation of neurons in the developing mammalian nervous system. We have previously shown that mutations in the β-tubulin gene *TUBB5* cause microcephaly with structural brain abnormalities in humans. While it is known that TUBB5 is necessary for the proper generation and migration of neurons, little is understood of the role it plays in neuronal differentiation and connectivity. Here, we report that perturbations to *TUBB5* disrupt the morphology of cortical neurons, their neuronal complexity, axonal outgrowth, as well as the density and shape of dendritic spines in the postnatal murine cortex. The features we describe are consistent with defects in synaptic signaling. Cellular-based assays have revealed that TUBB5 substitutions have the capacity to alter the dynamic properties and polymerization rates of the microtubule cytoskeleton. Together, our studies show that TUBB5 is essential for neuronal differentiation and dendritic spine formation *in vivo*, providing insight into the underlying cellular pathology associated with TUBB5 disease states.**

## INTRODUCTION

Cerebral cortical development relies on a step-wise process of neurogenesis, cell migration and terminal differentiation as neurons are added to the growing fetal brain (for reviews, see 1,2). Following their birth within the germinal zones new neurons must coordinate their cell shape in order to engage in movement, enabling them to reach their assigned positions within the cerebral cortical anlage (3,4). Once their positions have been finalized, postmigrational cortical neurons undergo extensive morphological changes forming dendritic trees and extending their axons, as they make contacts with other neurons through the formation of dendritic spines (5,6). The dynamic properties of the neuronal cytoskeleton provide immature neurons with the capacity to alter their morphology in the course of their migration and differentiation (1,2,7).

The importance of the microtubule cytoskeleton in the development of the cerebral cortex is reflected by the finding that mutations in a number of alpha and beta tubulins are responsible for a range of neurodevelopmental disorders (8). For instance, mutations in TUBA1A, TUBB2B and TUBB3 cause a spectrum of cortical abnormalities that include lissencephaly, polymicrogyria-like malformations and an ocular motility disorder (9–13). Similarly, functional studies employing genetically modified mice, as well as *in vivo* gene perturbations, have demonstrated that disruption of *TUBA1A*, *TUBB2A*, *TUBB2B* and *TUBB3* can result in defects in neuronal migration (12–16). These studies have revealed that mutations in the tubulin genes can interfere with the dynamic properties of the cytoskeleton, including its polymerization, stability and association with microtubule-associated proteins such as Kif21a (13). We recently reported that the β-tubulin gene *TUBB5* (also known as *TUBB*, Refseq

*To whom correspondence should be addressed. Email: julian.heng@monash.edu; david.keays@imp.ac.at
†L.N. and M.H. contributed equally to this study.

Gene ID:203068) is highly expressed in neuronal progenitors and postmitotic neurons during fetal cortical development in mice and humans (17). Furthermore, we described three human patients with amino acid substitutions to the TUBB5 polypeptide sequence (M299V, V353I and E401K), who present with structural brain disorders and cognitive deficits. While it is known that *in vivo* perturbation of *Tubb5* can alter the mitotic index of progenitor cells and their subsequent migration within the embryonic mouse cortex (17), it is unclear what role TUBB5 plays with respect to the differentiation and connectivity of neurons within the postnatal cortex. In this study, we address this question by employing *in utero* electroporation to study the function of *Tubb5* during neuronal differentiation. We report alterations in cell morphology, dendritic spine density, neuronal complexity and axon outgrowth in the mouse cerebral cortex, following the depletion of *Tubb5*, or expression of the disease-causing variants. We further demonstrate that perturbation of TUBB5 alters the dynamic properties of the microtubule cytoskeleton, highlighting its function within cells during neurodifferentiation.

## RESULTS

### Tubb5 perturbation alters the morphology of cells within the embryonic cerebral cortex

Within the embryonic cerebral cortex, newborn neurons in the ventricular zone (VZ) undergo extensive changes to their morphology as they transit within the intermediate zone (IZ) before engaging in radial migration to reach their appropriate positions within the cortical plate (CP) (reviewed in 3,18). We asked if Tubb5 directly influenced the morphological characteristics of embryonic cortical neurons, by performing *in utero* electroporation experiments at E14.5 with a previously validated *Tubb5* shRNA vector (17) together with a GFP expression cassette to identify electroporated cells (19) (Fig. 1A). We then analyzed the morphological properties of these postmitotic cortical neurons 3 days following electroporation (at E17.5), paying particular attention to their shape. Within the IZ of *Tubb5* shRNA-treated cortices, there was a significant decrease in the proportion of multipolar-shaped cells compared with control cortices, with a corresponding increase in the proportion of round-shaped cells which lacked processes, or have very short processes (Fig. 1A and C; 17.94% $\pm$ 1.52% multipolar cells in *Tubb5* shRNA treatment compared with 26.40% $\pm$ 1.14% in control; and 17.74% $\pm$ 1.78% round cells in the with 6.83% $\pm$ 0.88% in control; $F_{2,27} = 14.05$; two-way ANOVA followed by Bonferroni's *post hoc* test). The proportion of uni/bipolar-shaped cells was not altered (Fig. 1C). Within the CP, we detected an increase in the proportion of round-shaped cells, and a corresponding decrease in uni/bipolar-shaped cells (Fig. 1A and B; 17.27 $\pm$ 1.15% round cells in *Tubb5* shRNA treatment compared with 7.43% $\pm$ 1.40% in control; and 82.47 $\pm$ 1.10% uni/bipolar-shaped cells in *Tubb5* shRNA treatment compared with 92.57 $\pm$ 1.40% in control; $F_{2,27} = 44.77$; two-way ANOVA followed by Bonferroni's *post hoc* test). In addition to these changes in cell shape, we observed that the length of the leading processes of GFP-labeled cells was significantly decreased upon *Tubb5* knockdown (Fig. 1D and E). Therefore, suppression of *Tubb5* significantly alters the morphology of migrating neurons within the embryonic cerebral cortex.

Forced expression of the pathogenic variants M299V, V353I and E401K [but not wild-type TUBB5, denoted as TUBB5(WT)] impairs cell migration within the embryonic cortex (17). Hence, we analyzed embryonic cortices electroporated with expression constructs for TUBB5 and its variants M299V, V353I and E401K to uncover possible effects on the morphology of migrating neurons *in vivo*. We began by analyzing the morphological profiles of neurons overexpressing TUBB5(WT) compared with control treatment in which neurons express endogenous Tubb5. Surprisingly, we found that forced expression of TUBB5(WT) resulted in a decrease in multipolar-shaped neurons and a concomitant increase in the proportion of uni/bipolar-shaped neurons within the IZ (Fig. 2A–C, 14.2 $\pm$ 2.08% multipolar neurons in TUBB5(WT) versus 26.4 $\pm$ 1.13% in control; and 79.24 $\pm$ 1.72% uni/bipolar neurons in TUBB5(WT) versus 66.76 $\pm$ 0.77% in control $F_{8,60} = 18.03$; two-way ANOVA followed by Bonferroni's *post hoc* test) but the morphologies of neurons within the CP were not affected (Fig. 2B). This result indicated that forced expression of TUBB5(WT) alters the morphology of embryonic cortical neurons in a manner which is different to *Tubb5* knockdown. We also found that each pathogenic TUBB5 variant significantly affected the morphologies of the migrating neurons in different ways. Within the IZ, we found that forced expression of all three variants resulted in the suppression of multipolar morphologies; treatment with M299V led to an increase the proportion of uni/bipolar-shaped neurons; treatment with V353I increased the proportion of round-shaped cells; and treatment with E401K mutant increased the proportions of both round-shaped cells and uni/bipolar cells (Fig. 2C). In the CP, treatment with all three missense variants of TUBB5 induced round-cell shapes while suppressing uni/bipolar morphologies (Fig. 2B). Furthermore, GFP-positive cells transfected with E401K were found to have shorter leading neurites compared with control (Fig. 2D and E). Together, these results demonstrate that perturbations to TUBB5 alter the morphologies of embryonic neurons within the E17.5 cortex, which might contribute to their defective migration as previously reported (17).

### TUBB5 perturbation alters the neuronal complexity and axon outgrowth of postnatal (P17) cerebral cortical neurons *in vivo*

We investigated the consequences of *Tubb5* knockdown on the morphology of differentiated neurons within the postnatal (P17) cortex which were co-labeled with GFP protein expression at E14.5. To do this, we combined high-power microscopy with 3D computer reconstruction to analyze the morphology (Fig. 3; Supplementary Material, Fig. S1) of layer II/III cortical neurons. We then investigated their dendritic complexity by performing Sholl analysis as a means of representing the branching characteristics of neurons with increasing distance from the cell body (20). We found that *Tubb5*-deficient neurons display a more complex morphology adjacent to the cell body (Supplementary Material, Fig. S2A; analysis of co-variance (ANCOVA) for the region defined as 3–35 μm from the soma; $P < 0.001$), as well as a simplified morphology away from the cell (Supplementary Material, Fig. S2A; ANCOVA for the region defined as 40–65 μm from the soma; $P < 0.001$). When we investigated

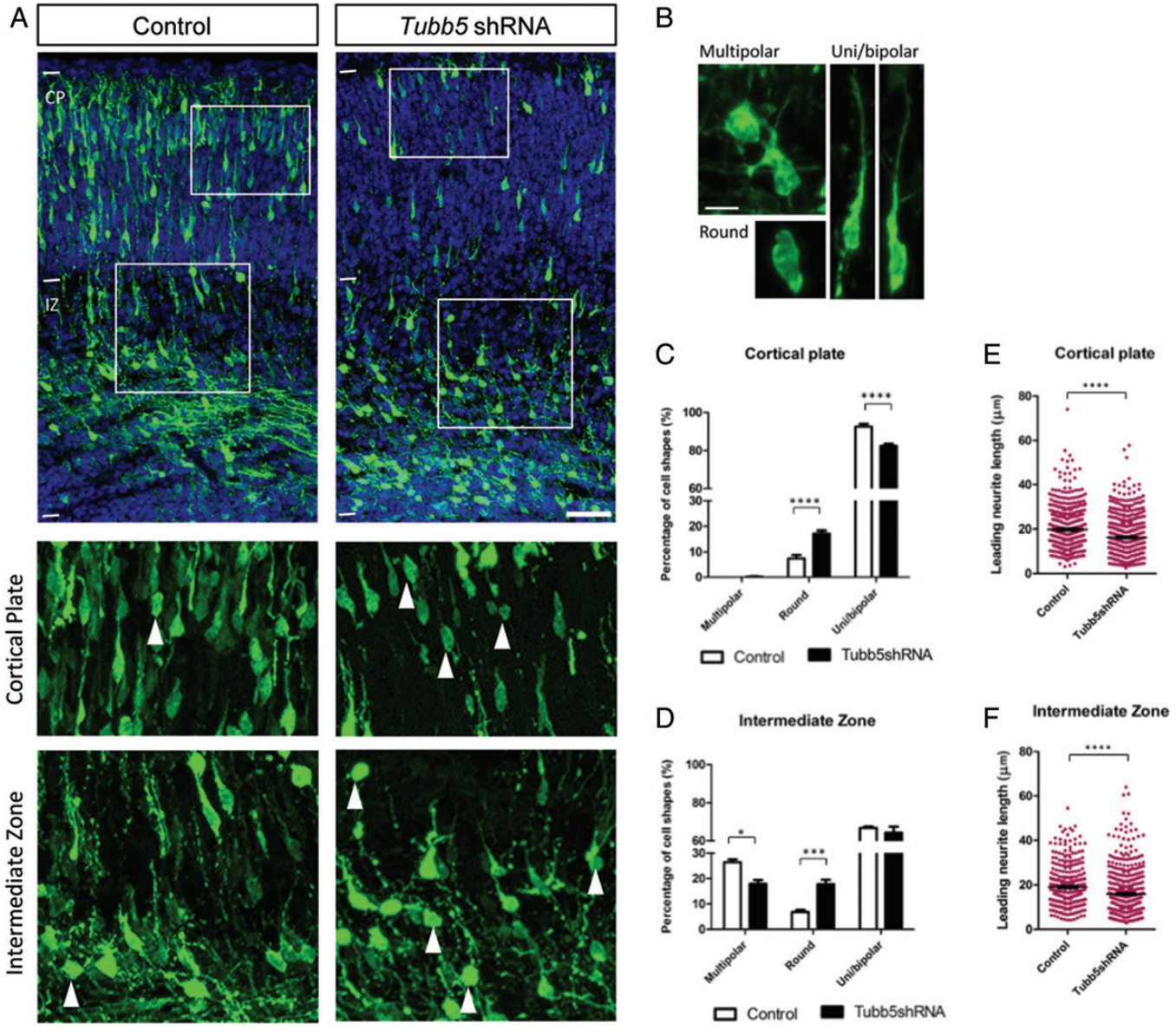


**Figure 1.** Knockdown *of Tubb5* alters the morphology of migrating neurons. (**A**) Representative images of E17.5 cortices electroporated with control and *Tubb5* shRNA plasmids together with GFP at E14.5. Boxed inserts illustrate the morphology of GFP-labeled neurons within the CP and IZs of the embryonic cortex, with arrowheads pointing to round cells which either lack processes or have very short processes. (**B**) Representative images of multipolar, round and uni/bipolar-shaped neurons identified in our cell shape analysis. (**C**) *Tubb5* knockdown significantly increased the percentage of round-shaped cells and decreased the percentage of uni/bipolar-shaped cells within the CP (n: control = 515 cells, *Tubb5*shRNA = 563 cells). (**D**) Treatment with *Tubb5* shRNA significantly decreased the percentage of multipolar cells, and significantly increased the percentage of round-shaped cells in the IZ compared with control (n: control = 455 cells, *Tubb5*shRNA = 717 cells). (**E** and **F**) The leading neurites of *Tubb5* shRNA-treated uni/bipolar neurons within the CP and IZ were significantly shorter than the neurite lengths of control cells within the E17.5 mouse cortex (n: control = 705 cells, *Tubb5*shRNA = 840 cells); $^{*}P < 0.05$, $^{**}P < 0.01$, $^{***}P < 0.001$ and $^{****}P < 0.0001$. Scale bar: (A), 100 μm; (B), 10 μm.

the nature of the change in Sholl profile, we found that the neurites of *Tubb5*-deficient neurons were more branched, but the numbers of primary neurites were not significantly increased, despite a trend (Fig. 3A–D; $n = 21$ and 22 for control and *Tubb5* shRNA treatment, respectively). Furthermore, we observed a reduction in GFP-labeled callosal axons within P17 cortices treated with *Tubb5* shRNA compared with control shRNA (Supplementary Material, Fig. S2B).

Next, we investigated the effects of expressing TUBB5(WT) and its pathogenic variants on the dendritic complexity of P17 projection neurons (Fig. 4). We found that forced expression of TUBB5(WT) increased the complexity of neurons compared with control (GFP only). Interestingly, when we compared the profile of TUBB5-overexpressing neurons with those treated with M299V, V353I and E401K construct, it would appear that all three pathogenic variants have lost the ability to enhance dendritic complexity (Fig. 4B). We observed a severe reduction in the complexity profile of neurons treated with M299V or E401K (Supplementary Material, Fig. S6A and B), while the profile of V353I-expressing neurons was more

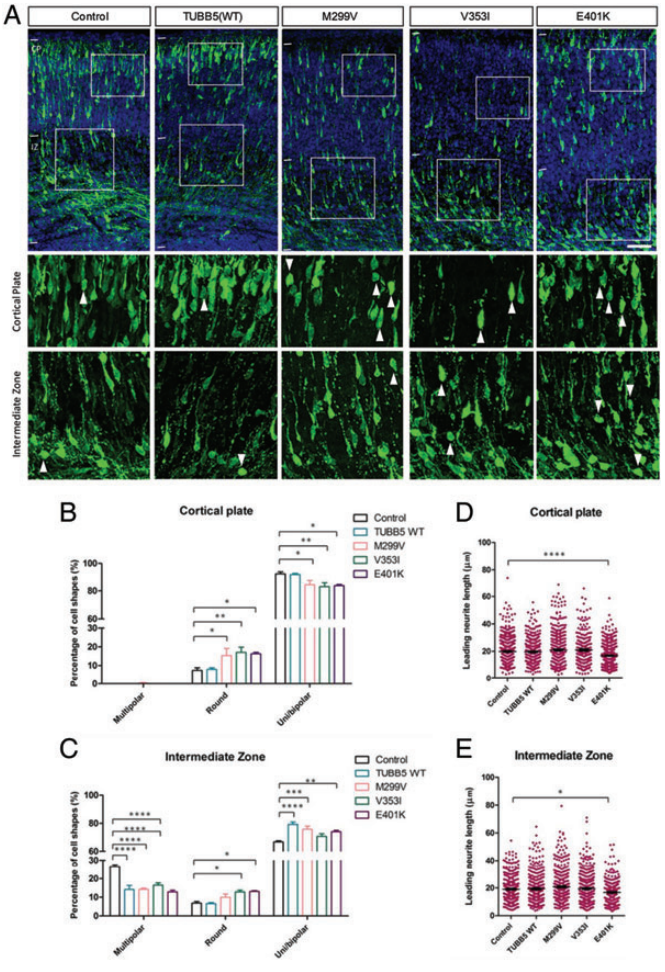


**Figure 2.** TUBB5 alters the morphology of migrating neurons. (**A**) The morphological profiles of the migrating neurons within the E17.5 mouse cortex following treatment with either control vector or TUBB5(WT) or its pathogenic variants. Boxed inserts illustrate the morphology of neurons within the CP and IZs, with arrowheads pointing to round-shaped cells (**B** and **C**) Forced expression of TUBB5 and its variants significantly altered the shapes of neurons within the embryonic E17.5 cortex (n: control = 515 cells, TUBB5(WT) = 428 cells, M299V = 473 cells, V353I = 401 cells, E401K = 488 cells for CP analysis; n: control = 455 cells, TUBB5(WT) = 406 cells, M299V = 490 cells, V353I = 620 cells, E401K = 510 cells for intermediate zone analysis). (**D** and **E**) E401K-treated neurons presented with significantly shorter leading neurites compared with the control treatment (n: control = 475 cells, TUBB5(WT) = 403 cells, M299V = 410 cells, V353I = 253 cells, E401K = 409 cells for CP analysis; n: control = 357 cells, TUBB5(WT) = 357 cells, M299V = 376 cells, V353I = 414 cells, E401K = 378 cells for IZ analysis), $^{*}P < 0.05$, $^{**}P < 0.01$, $^{***}P < 0.001$ and $^{****}P < 0.0001$. Scale bar: 100 μm.

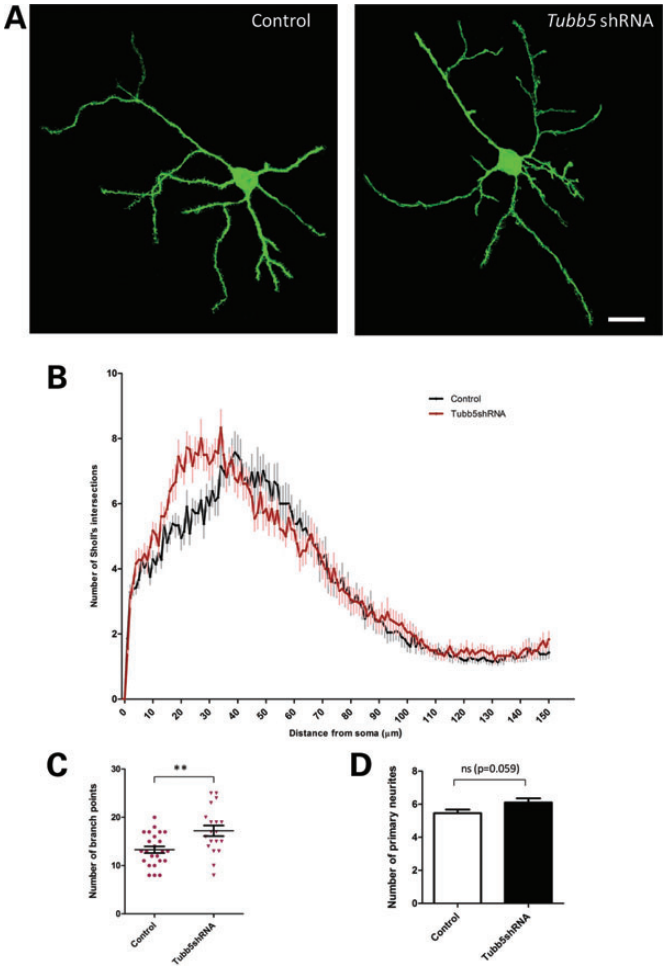


**Figure 3.** Knockdown of *Tubb5* leads to altered dendritic arborization of layer II/III projection neurons within the P17 mouse cerebral cortex. (**A**) Representative 3D images of layer II/III projection neurons following control and *Tubb5* shRNA treatment at P17. (**B**) Sholl analysis revealed an altered dendritic arbor complexity of *Tubb5* shRNA-treated neurons (18 cells analyzed) compared with controls (21 cells analyzed). (**C**) The dendritic trees of *Tubb5* shRNA-treated neurons have significantly more branch points compared with controls; $P = 0.005$. (**D**) The number of primary neurites was not significantly different between control and *Tubb5* shRNA treatment; $P = 0.059$. Student's unpaired *t*-tests, $^{*}P < 0.05$, $^{**}P < 0.01$. Scale bar: 30 μm.

similar to the control (Fig. 4B). We found that forced expression of TUBB5 and its missense variants did not significantly alter neurite branching or the number of primary neurites compared with control treatment (Fig. 4C and D, $P > 0.05$ Bonferroni's multiple comparisons test). We additionally analyzed callosal axon outgrowth and detected the presence of GFP-labeled fibers in 100% of brains electroporated with control vector (five out of five brains), TUBB5(WT) (three out of three brains), as well as the variant M299V (five out of five brains). In contrast, we observed a weak effect of E401K transduction (three out of four brains) on the presence of GFP-labeled callosal axons, while GFP-labeled axons were not detected in 100% of brains (three out of three brains) electroporated with V353I construct (Supplementary Material, Fig. S3). Together, these results demonstrate that perturbations to TUBB5 alter the morphology of cortical projection neurons within the postnatal cortex.

## TUBB5 and its pathogenic variants alter the numbers and shapes of dendritic spines

To explore whether TUBB5 depletion influenced the densities of dendritic spines, we combined GFP-imaging with 3D image reconstruction (Supplementary Material, Fig. S4) and analyzed the dendrites of layer II/III neurons. We performed separate analyses on apical and basal dendrites since both have different properties and can respond differently to signaling molecules

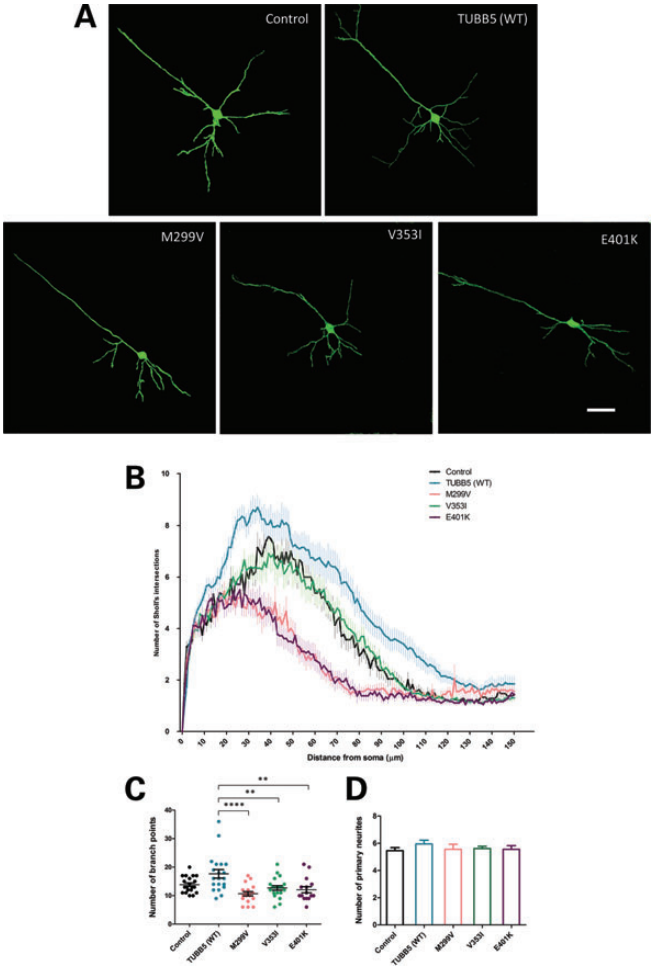


**Figure 4.** TUBB5 and its pathogenic variants alter the dendritic complexity of layer II/III cortical projection neurons within the P17 mouse cortex. (**A**) Representative 3D images of layer II/III projections following treatment with control vector, TUBB5 WT or its pathogenic variants. (**B**) Sholl analysis revealed a global reduction in the complexity of neurons treated with M299V or E401 K constructs (18 cells analyzed), whereas the dendritic arbor complexity of TUBB5 WT-expressing cells was enhanced compared with control (>20 cells analyzed per condition). (**C** and **D**) When compared with neurons treated with TUBB5(WT) vector, expression of each of the three pathogenic variants led to a reduction in neurite branching, but the number of primary neurites was not significantly different. $P > 0.05$. Scale bar: 30 µm.

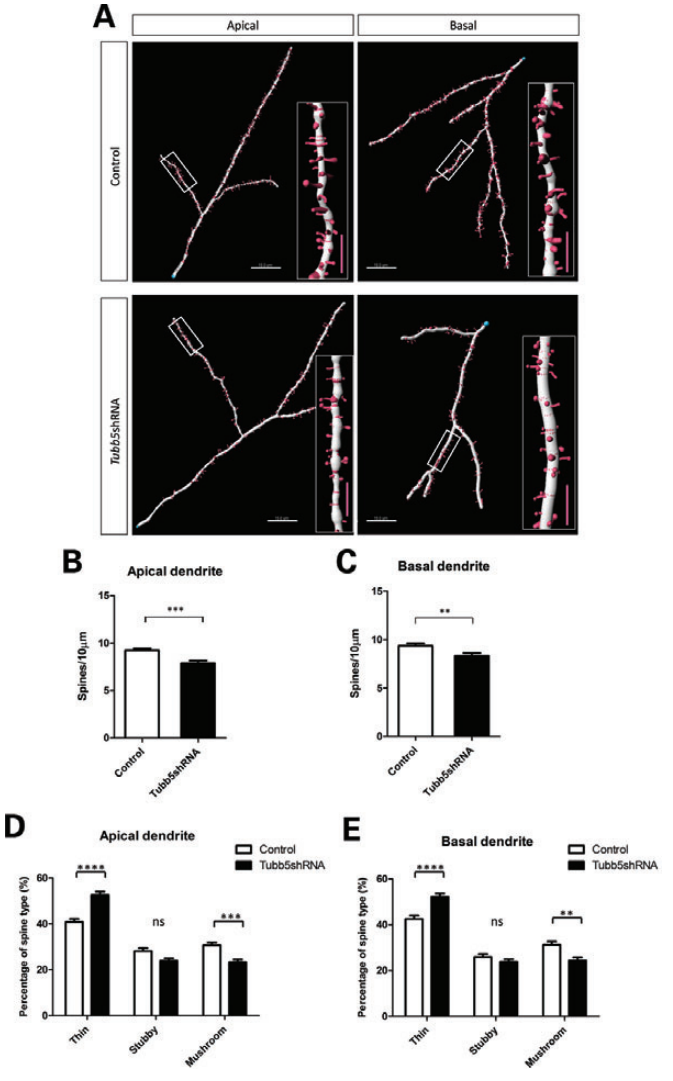


**Figure 5.** Altered dendritic spine densities and spine morphologies of layer II/III cortical projection neurons within the P17 mouse cortex following *Tubb5* depletion. (**A**) Representative 3D images of apical and basal dendrites of control and *Tubb5* shRNA-treated neurons. (**B** and **C**) Knockdown of *Tubb5* significantly reduced the spine density in both apical ($P = 0.0004$) and basal dendrites ($P = 0.01$) compared with controls (>20 apical or basal dendrites analyzed for each condition). GFP-imaged neurons are illustrated in Supplementary Material, Figure S7 (**D** and –**E**) *Tubb5* knockdown significantly altered the proportion of thin and mushroom-shaped spines on both apical ($F_{2,108} = 31.16$; $P < 0.0001$) and basal dendrites ($F_{2,104} = 18.39$; $P < 0.0001$) compared with controls. $^{**}P < 0.01$, $^{***}P < 0.005$. White scale bars: 15 µm; red scale bars in insets: 5 µm.

(21). Our results show that *Tubb5* knockdown results in a significant decrease in the total number of dendritic spines in the apical and basal dendrites of cortical neurons (Fig. 5A–C). We also observed that these decreases in spines densities occurred along the lengths of both types of dendrites (Supplementary Material, Fig. S5). We further classified dendritic spine morphologies into thin, stubby and mushroom-shaped protrusions as morphological correlates of their synaptic signaling properties (reviewed in 22). Our statistical analysis revealed that *Tubb5*-deficient neurons displayed a significant increase in the proportion of thin spines, and a concomitant reduction in the proportion of mushroom-shaped spines, while the proportion of stubby spines was not altered in both apical and basal dendrites (Fig. 5D and E). Hence, *Tubb5* is required for correct dendritic spine densities as well as spine morphology on postnatal cortical neurons.

We also wanted to determine if TUBB5 and its pathogenic variants influenced the dendritic spines of cortical neurons. We found treatment with the M299V variant resulted in a significant reduction in the density of dendritic spines across the lengths of apical and basal dendrites (Fig. 6A–D; Supplementary Material, Fig. S6C and D); while expression of the V353I and E401K mutants, or TUBB5(WT) did not have an effect. When we analyzed the morphologies of dendritic spines, we observed a

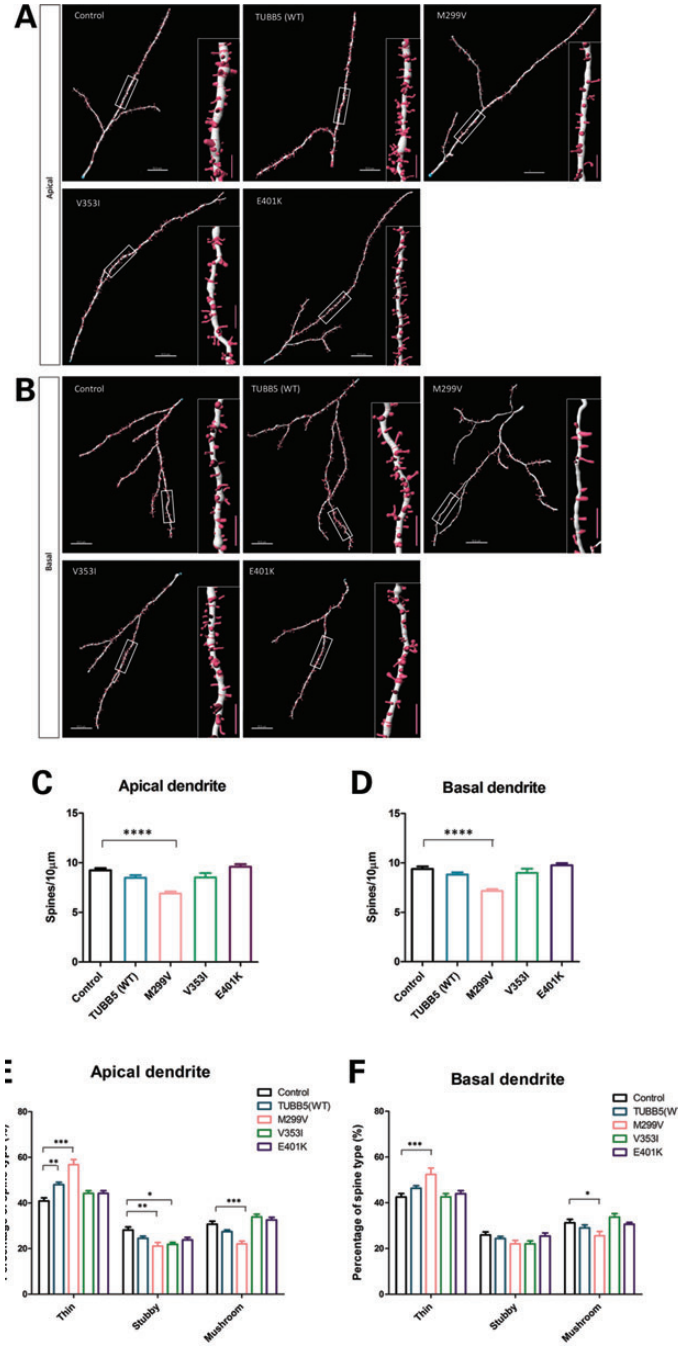


**Figure 6.** Altered dendritic spine density and spine morphology of layer II/III projection neurons within the P17 cortex following overexpression of TUBB5. (**A** and **B**) Representative 3D images of apical and basal dendrites of layer II/III projections neurons expressing TUBB5(WT) or its pathogenic variants. (**C** and **D**) The M299V variant caused a significant decrease in spine density on both apical and basal dendrites compared with controls (20 apical and basal dendrites analyzed for controls; 20 apical and 17 basal dendrites analyzed for M299V; $P < 0.0001$). In contrast, overexpression of TUBB5(WT), V353I and E401K did not significantly alter the dendritic spine densities of layer II/III neurons compared with controls. GFP-imaged neurons are illustrated in Supplementary Material, Figure S7. (**E** and **F**) Forced expression of the M299V variant resulted in extensive changes to spine types on both apical and basal dendrites of layer II/III projection neurons. $^{*}P < 0.05$, $^{**}P < 0.01$, $^{***}P < 0.005$ and $^{****}P < 0.0001$. White scale bars: 15 μm; red scale bars in insets: 5 μm.

significant increase in the proportion of thin spines in both the apical and basal dendrites of M299V-expressing neurons, with concomitant decreases in stubby and mushroom spines (Fig. 6E and F). On the other hand, forced expression of the V353I variant resulted in a significant decrease in the proportions of stubby spines, while a significant increase in the proportion of thin spines was detected in neurons upon forced expression of TUBB5(WT) (Fig. 6E). Therefore, our results demonstrate that TUBB5 and its pathogenic variants have divergent effects on the dendritic spine densities and morphologies of P17 cortical projection neurons.

## TUBB5 is important for the dynamic polymerization properties of the microtubule cytoskeleton

Given the effects on cortical neuron differentiation, we asked whether disruptions to *Tubb5* expression alter the dynamic properties of the microtubule cytoskeleton. We began by studying the effects of *Tubb5* RNAi on microtubule dynamics via co-transfection of an expression construct encoding GFP-tagged EB3, a microtubule end-binding protein (23). In Neuro2A cells treated with *Tubb5* shRNA, we found that the velocity of EB3 'comets' was significantly reduced when compared with control treatment (scrambled shRNA vector), but this was rescued when *Tubb5* shRNA-treated cells were co-transfected with a wild-type TUBB5 expression construct (Fig. 7A and B). Since the decreased velocity of EB3 comets in *Tubb5* shRNA-treated cells might indicate a decrease in microtubule growth (23,24), we performed a second experiment to study the effect of *Tubb5* RNAi on the repopulation of the microtubule meshwork in Neuro2A cells following treatment with nocodazole, a drug which interferes with microtubule polymerization (24). When we plotted the proportion of cells with an intact microtubule meshwork for up to 20 min following withdrawal of nocodazole in the culture media, we observed an impairment of meshwork formation in *Tubb5* shRNA-treated cells (Fig. 7C and D; $F_{2,47} = 4.869$; $P = 0.012$, two-way ANOVA). Particularly, the proportion of cells with an intact microtubule meshwork was significantly decreased 10 min after nocodazole-containing media was replaced with drug-free media, but this deficit was corrected by 20 min. In addition, we found that the altered meshwork phenotype of *Tubb5* shRNA-treated cells could be restored by co-transfected of a wild-type TUBB5 construct (Fig. 7C and D).

Since our RNAi studies indicated that changes to *Tubb5* levels disturb microtubule dynamics, we predicted that forced expression of TUBB5 would likely affect the microtubule cytoskeleton as well. To address this, we measured GFP-EB3 comet velocities of cells transfected with expression constructs encoding TUBB5(WT), or the variants M299V and V353I which are both competent for assembly into microtubules (17). We found that forced expression of TUBB5(WT), M299V and V353I in cells resulted in a significant increase in EB3 comet velocities compared with control treatment (Fig. 8A). In contrast, two interesting observations were made in cells transfected with E401K, a variant which does not incorporate into the microtubule network (17). Firstly, we observed that comet velocities were significantly reduced in E401K-treated cells compared with TUBB5(WT) (Fig. 8A, $0.256 \pm 0.006$ μm/s versus

0.368 ± 0.011 μm/s; $P < 0.0001$; Bonferroni's *post hoc* test). Secondly, the comet velocities of E401K-treated cells were not significantly different to control (Fig. 8A; 0.256 ± 0.006 μm/s versus 0.291 ± 0.008 μm/s; $P > 0.05$; Bonferroni's *post hoc* test). Thus, it would appear that the effect of forced expression of TUBB5 on GFP-EB3 comet velocities in cells is a function of its capacity to incorporate into the microtubule cytoskeleton.

To study how the TUBB5 variants might influence microtubule polymerization in cells, we transfected Neuro2A cells with expression constructs encoding TUBB5(WT), M299V, V353I or E401K and examined their effects on microtubule meshwork formation following nocodazole treatment (Fig. 8B). Our results show that forced expression of the V353I variant impaired microtubule meshwork formation compared with control (expression vector only), while meshwork formation was not significantly different with TUBB5(WT), M299V and E401K. Taken together, these results demonstrate that perturbations to TUBB5 disrupt the microtubule cytoskeleton of cells, including the trafficking of EB3 as well as the formation of an intact meshwork.

## DISCUSSION

In this study, we have investigated the role of TUBB5 in neuronal differentiation and connectivity. We show that perturbations to *TUBB5* disrupt the morphology of cortical neurons, axonal outgrowth, as well as the density and shape of dendritic spines in the postnatal murine cortex.

The dynamic properties of the microtubule cytoskeleton are crucial for the morphological changes that occur as a neuron extends its leading process, retracts its trailing process and translocates its nucleus in order to migrate (1,2,7). Within the IZ of the embryonic cortex, neurons engage in a multipolar-to-bipolar transition as they move into the CP, and we find that a reduction in *Tubb5* expression results in an increase in the percentage of round cells in theIZ, concomitant with a decrease in the percentage of multipolar cells. This contrasts with the effects of forced expression of native TUBB5 that leads to a reduction in the percentage of multipolar cells within theIZ, but with an increase in uni/bipolar-shaped neurons. In further support for a direct role for TUBB5 in neuronal shape acquisition, we demonstrate that forced expression of the pathogenic variants of TUBB5 also leads to a decrease in multipolar cells within the IZ, with corresponding increases in the proportions of round and/or bipolar-shaped cells. In the CP where uni/bipolar-shaped neurons locomote along radial glial fibers (25), we find that perturbations to TUBB5 disrupt the acquisition of a uni/bipolar morphology. In addition, *Tubb5* knockdown or expression of the E401K variant leads to a decrease in the length of the leading process. It is therefore apparent that perturbations to *TUBB5* disrupt the morphological transitions undertaken by neurons as they migrate from the VZ into the CP, which may contribute to the delay in neuronal migration we have previously reported (17) (summarized in Fig. 9). This conclusion is supported by a recent study from Chelly and colleagues which showed that suppression of the β-tubulin gene *Tubb3* disrupts radial migration, resulting in an accumulation of round-shaped cells within the lower IZ and SVZ of the embryonic E18.5 mouse cerebral cortex (16). Taken together, our

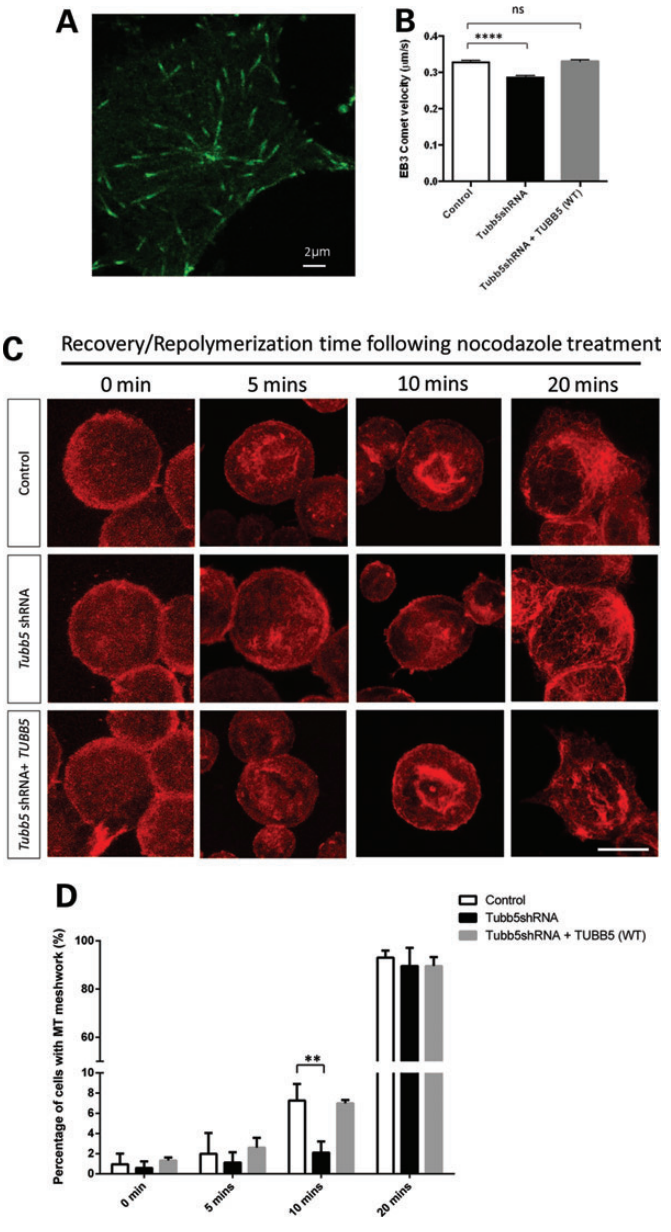


**Figure 7.** The effects of *Tubb5* RNAi on the microtubule cytoskeleton of cells. (**A**) Visualization of EB3 comets within Neuro2A cells. (**B**) Knockdown of *Tubb5* significantly decreased the average trafficking velocities of EB3 comets in Neuro2A cells compared with control, and this effect was rescued with co-delivery of a wild-type TUBB5 expression construct (100 comets measured from at least five cells per condition, $^{****}P < 0.0001$ unpaired *t*-test). (**C** and **D**) Confocal images of Neuro2A cells immunostained for α-tubulin document the dispersed microtubule cytoskeleton of cells and absence of meshwork following nocodazole treatment (0 min in drug-free media). When control-treated cells were incubated in drug-free media for 5 min, we observed a condensation signal consistent with reformation of the microtubule meshwork, and this signal which intensified after 10 min coincided with the presence of inter-connected strands of α-tubulin immunostained fibers. The MT meshwork of cells is clearly visible by 20 min. In contrast, there is a significant reduction in the proportion of *Tubb5* shRNA-treated cells with a visible meshwork after 10 min, and we found that cells had a notable decrease in MT condensation ($F_{2,47} = 4.869$; $P = 0.012$; two-way ANOVA). However, by 20 min in drug-free media, the proportion of cells with meshwork was not significantly different between conditions. We found that the reduction in meshwork formation in *Tubb5* shRNA-treated cells could be rescued by co-delivery of a wild-type TUBB5 expression construct. Scale bars: (**A**) 2 μm; (**C**) 10 μm.

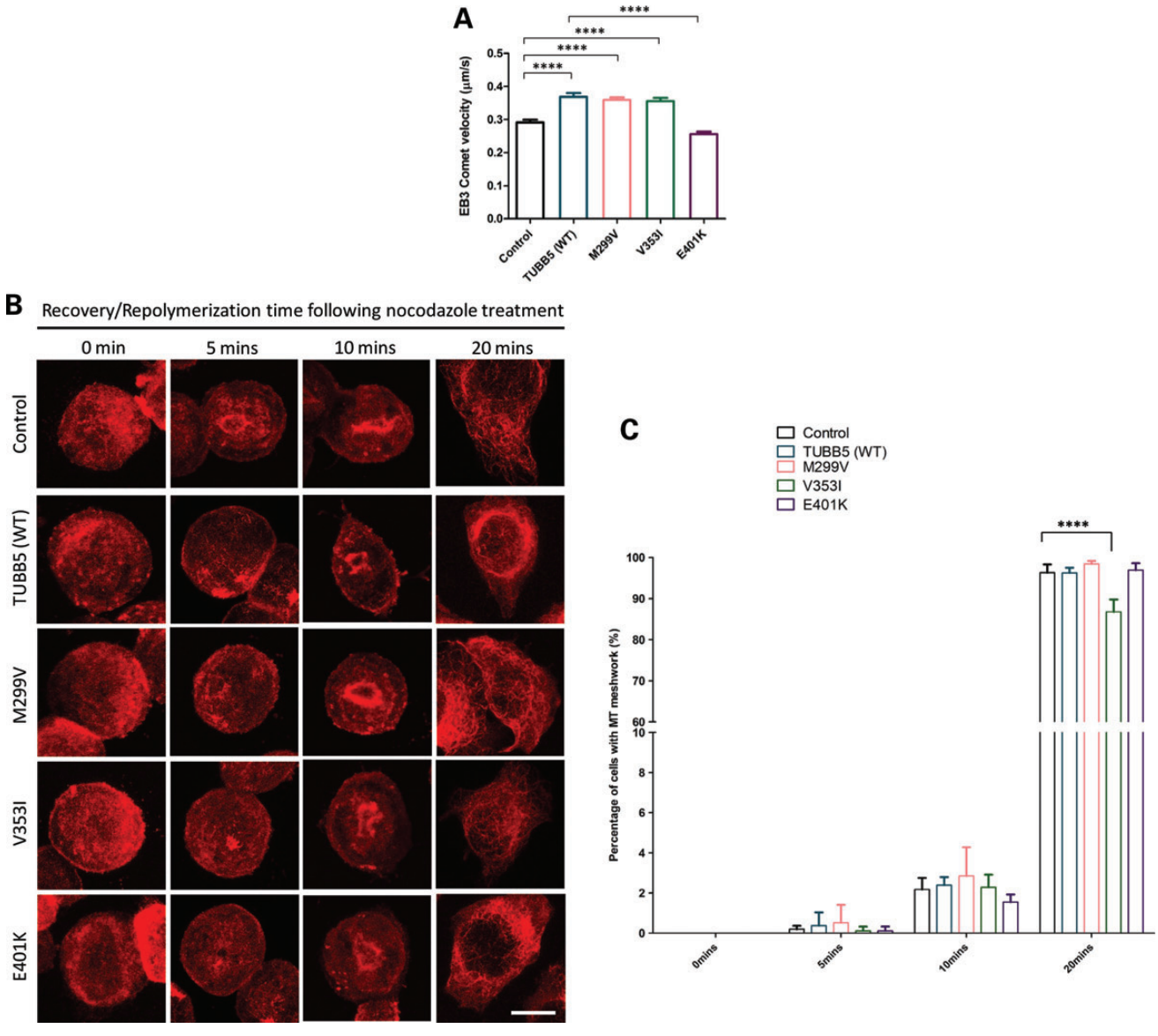


**Figure 8.** The effects of TUBB5 and its pathogenic variants on the microtubule cytoskeleton. (**A**) There was a significant increase in the velocities of EB3 comets tracked within Neuro2A cells transfected with TUBB5(WT), M299V and V353I, when compared with control. In contrast, comet velocities recorded in E401K-treated cells were significantly different to TUBB5(WT)-treated cells ($P < 0.0001$), but not to control ($P > 0.05$). (**B**) Photomicrographs depicting Neuro2A cells transfected with TUBB5 and its variants, and analyzed for the formation of microtubule meshwork following nocodazole treatment. (**C**) While forced expression of TUBB5(WT), M299V and E401K did not significantly disrupt meshwork reformation in this assay, we found that treatment with the V353I variant resulted in a significant decrease in the proportion of cells which comprised an intact meshwork 20 min after nocodazole clearance ($F_{12,40} = 14.19$, $P < 0.0001$; two-way ANOVA followed by Bonferroni's *post hoc* test with multiple testing correction). Scale bar: 10 μm.

studies are consistent with the notion that the tubulins are critical to the morphology and migration of immature neurons during cortical development.

It is known that the dynamic stability of microtubules also influences the elaboration of dendrites and axons (2,5), and we find that perturbations to TUBB5 disrupt dendritic branching of cortical projection neurons within the postnatal cortex. Moreover, *Tubb5* shRNA treatment, as well as forced expression of the V353I variant disrupts the outgrowth of callosal axons within the postnatal cortex. In support of a specific role for Tubb5 in vertebrate axonogenesis, a recent study by Baraban and colleagues reported distinct axonal localization of *Tubb5* mRNA transcripts within embryonic neurons in zebrafish (26). In addition to these cell intrinsic functions for TUBB5 in controlling cell shape, the microtubule cytoskeleton also provides a substrate for the trafficking of essential substrates and growth factor receptors to and from the cell periphery to regulate process outgrowth in response to signaling factors in the tissue environment,

such as IGF-1 (27). Hence, changes to TUBB5 could affect the growth and structural integrity of the microtubule cytoskeleton, as well as microtubule-associated trafficking of receptor molecules which, in turn, influences the dendritic growth and branching of postmitotic cortical neurons. Collectively, these documented changes in dendritic branching could alter the somatic versus dendritic connectivity of cortical projection neurons, leading to imbalances in excitatory and inhibitory tone which, in turn, trigger epileptogenesis (28,29).

Recently, it was discovered that the microtubule cytoskeleton plays an important role in shaping the actin network within nascent dendritic spines of hippocampal neurons so as to regulate their formation, morphology and synaptic signaling (30–32). Our study directly implicates TUBB5 in the formation of dendritic spines in the murine cortex. We observe a reduction in the proportion of mushroom-shaped spines, and a concomitant increase in the proportion of thin spines, when TUBB5 expression levels were suppressed by RNAi, or when the M299V mutant was introduced. Since thin spines display features consistent with immature synapses, while mushroom-shaped spines are more mature (reviewed in 22), these changes could suggest a delay or defect in spine development as a result of perturbations to TUBB5.

The abnormal cellular morphology, defects in axon guidance and dendritic spine phenotypes are likely to be associated with defects in the dynamism and/or polymerization of microtubules. In support of this notion, we find that suppression of *Tubb5* leads to a decrease in trafficking velocities of the microtubule end-binding protein EB3, which we interpret as a disruption to the growth of microtubules. This interpretation is consistent with our finding that suppression of *Tubb5* leads to a delay in the formation of the microtubule meshwork in cells following nocodazole treatment. Given that the stability of the microtubule meshwork influences the differentiation of immature neurons (33,34), it is tempting to speculate that changes to Tubb5 levels alter the polymerization of the neuronal microtubule network which, in turn, interferes with shape formation during neuronal differentiation.

Previous studies have shown that mutations to tubulins, such as TUBA1A and TUBB3, impair the migration of neurons, and can disrupt the polymerization of microtubules (12,13,17,24). Similarly, Tischfield and colleagues have reported that the R262C variant of TUBB3 which causes an ocular motility disorder, increases the stability of microtubules, alters their polymerization rates and reduces their association with the motor protein Kif21a (13). This contrasts with two mutations (T178M and E205K) in TUBB3 which cause cortical malformations that decrease the stability of microtubules (12). In these studies, Tischfield and Chelly employed primary cells harboring heterozygous mutations that mirror the genotype of patient causing mutations. As primary cell lines were not available in our case, we have relied on overexpression of the TUBB5 mutations in Neuro2A cells. While primary cells are clearly preferable, our work has nonetheless revealed that failure of the E401K mutation to incorporate into the microtubule cytoskeleton results in a reduction in the velocity of EB3 comets (in comparison to WT overexpression), and that the V353I mutation also disrupts microtubule meshwork formation induced by nocodazole treatment. Thus, our experiments have demonstrated an important difference in the polymerization properties of microtubules in the presence of the V353I variant compared with wild-type TUBB5. However, the generation of knockin mouse models will allow the detection of more subtle defects on microtubule dynamics and aid the identification of microtubule associated protein partners, such as Kif21a and Dcx (35–37), whose binding might be impaired by the presence of the M299V, V353I and E401K substitutions.

Taken together, our data strongly suggest that perturbations to TUBB5 have a deleterious effect on multiple aspects of neuronal differentiation within the murine cerebral cortex, including the maturation of dendritic spines. From our studies, we also predict that the presence of TUBB5 mutations in humans disrupts the connectivity and synaptic signaling of neurons. At this juncture it is not known whether mutations in other tubulins, such as TUBA1A, TUBB2A, TUBB2B and TUBB3, also result in abnormalities in spine density and shape (9–14). This may be of particular relevance to those tubulin mutations that have been implicated in autism-spectrum disorders, where no overt structural brain phenotypes have been reported (38,39).

## MATERIAL AND METHODS

### DNA plasmids and antibodies

DNA expression constructs used in this work have been reported (17). Primary antibodies used for immunostaining analysis include chicken polyclonal antibody to GFP (Abcam, ab13970, 1:700), mouse anti βIII-tubulin (Covance, MMS-435P, 1:1000), rabbit anti activated caspase3 (R&D Systems, AF835, 1:1000), rabbit polyclonal antibody to GFP (Invitrogen, A6455, 1:1000), rat monoclonal antibody to L1 (Millipore MAB5272, 1:400). Alexa fluor secondary antibodies include goat anti- chicken IgG (Invitrogen, A11039, 1:700), goat anti-mouse (Invitrogen, A11031, 1:800) and goat anti-rabbit IgG (Invitrogen, A6455, 1:1000). The nuclei of cells were visualized with DAPI.

### Animals

Mice were maintained within the animal facilities at Monash University. All animal procedures are approved by the Monash University Animal Ethics Committee (MARP/2012/068) and compliant with guidelines provided by the National Health and Medical Research Council of Australia.

### *In utero* electroporation

Time-mated pregnant (E14.5) C57B/6 female mice were anesthetized and the abdominal area was sterilized before the commencement of *in utero* electroporation. The abdominal cavity was accessed via a small incision, then the uterine horns were then gently exposed. One lateral ventricle of an embryonic (E14.5) mouse fetal forebrain was injected with a solution containing 1 μg/μl each of DNA expression plasmid encoding GFP, along with (i) an shRNA expression plasmid (either control or *Tubb5*-targeting shRNA) or (ii) a DNA expression plasmid encoding wild-type *TUBB5*, or its variants (M299V, V353I and E401K); together with tracer dye (Fast Green). Electroporation was carried out by a square-pulse generator as previously described (19). Following this, the uterine horns were returned to the abdominal cavity, and the peritoneal and skin

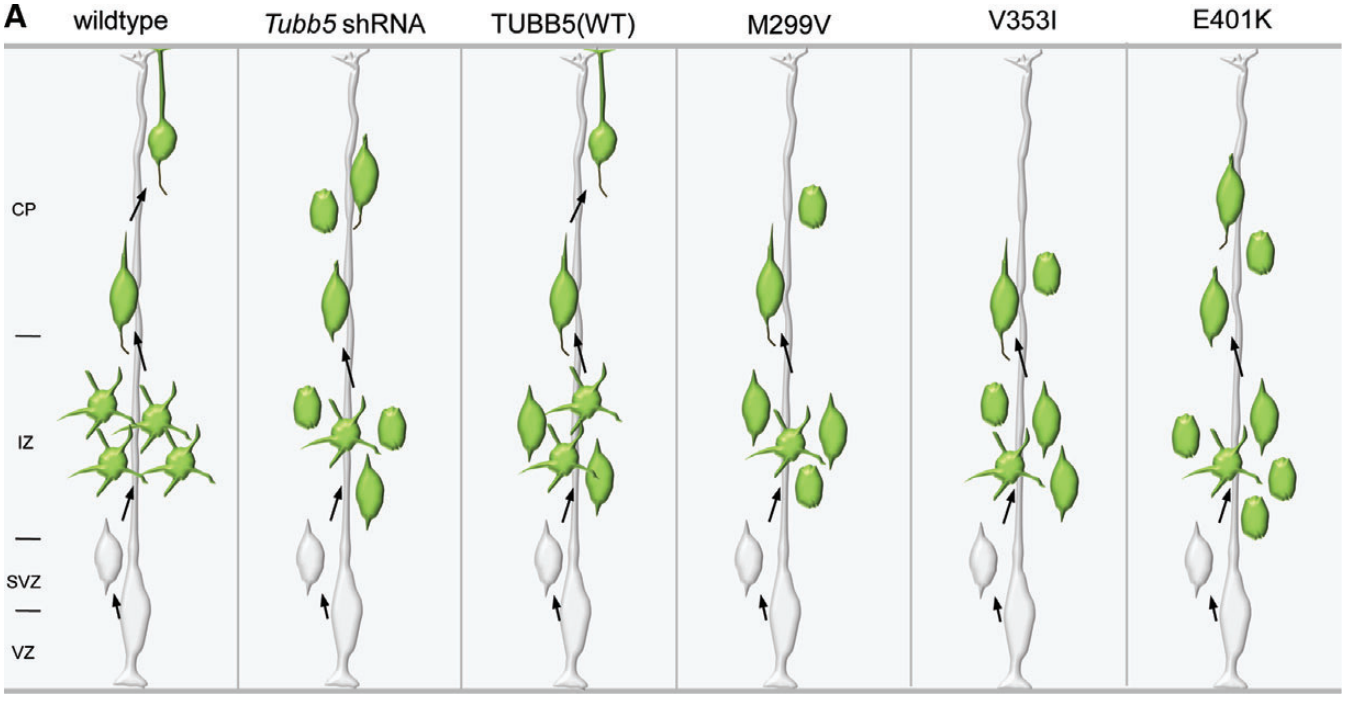


**Figure 9.** Summary scheme illustrating the effects of perturbations to TUBB5 on neuronal morphology and cell migration within the embryonic cerebral cortex. (**A**) As newborn cortical neurons leave the VZ and migrate towards the CP, they undergo distinct changes to their cell shape. Within the IZ, neurons adopt a multipolar morphology as they migrate towards the CP before they convert to a bipolar shape as they complete their migration through to the upper CP. Treatment of E14.5-born cortical cells with *Tubb5* shRNA results in their defective migration into the CP of E17.5 cortex. Cells fail to adopt a multipolar morphology, and there is an increase in the proportion of round cells and bipolar-shaped cells within the IZ. The leading processes of bipolar-shaped neurons are also decreased throughout the IZ and CP. Forced expression of TUBB5(WT) leads to a reduction of multipolar-shaped cells within the IZ, and an increase in bipolar-shaped cells, but their positioning within the embryonic cortex is not affected. However, forced expression of M299V, V353I and E401K leads to a migration defect, each with different effects on the morphology of neurons. For example, expression of M299V and V353I variants leads to a decrease in multipolar-shaped cells and an increase in the proportion of round cells and bipolar cells within the IZ. On the other hand, cells treated with E401K show defective morphologies within the IZ and CP, as well as a reduction in the length of the leading process of bipolar neurons. Green cells summarize findings presented in Figures 1 and 2.

was sutured. The mice were allowed to recover before embryos were collected 3 days later (at E17.5), or as pups maintained until postnatal Day 17 (P17) when brain tissue was harvested.

### Tissue processing and data acquisition

The brain samples were fixed in paraformaldehyde (4% in PBS) overnight at 4°C, then incubated for 3 days in PBS with 20% sucrose before embedding in OCT compound (Tissue-Tek®, USA) and cut with a cryostat to obtain 16 μm sections (E17.5 brains) or 40 μm sections (P17 brains) along a coronal plane. Immunohistochemistry was performed as previously described (40). Following immunostaining, digital images were acquired with an Imager.Z1 fluorescent microscope (Zeiss) or an Abrio C1 Upright (Nikon) confocal microscope and were processed with either Photoshop CS3 software (Adobe) or Fiji (ImageJ) software. Images from embryonic E17.5 cortices were acquired at ×20 magnification. Cell counting was performed blind to the condition on representative fields of sections of electroporated brains using ImageJ software. The boundaries between the VZ and SVZ, SVZ and IZ, and IZ and CP were determined based on the density of counterstained nuclei, as described previously (17,40). For the study of neuronal morphology and dendritic spines of GFP-labeled P17 neurons, confocal images were acquired at either ×40 or ×63 magnification, and as *z*-stack images with 1 μm steps. Digital image reconstruction of the morphologies of layer II/III cortical neurons was performed using Imaris. These cells were then subjected to Sholl analysis using MacBiophotonic ImageJ software, with the radii of Sholl circles defined for 150 μm, and at 1 μm intervals. For dendritic spine studies, unbiased counts were performed on z-stacked images using Neuronstudio software, with the following criteria for unbiased classifications for dendritic spines: minimum spine height is 0.3 μm; maximum spine height is 3.5 μm; maximum spine width is 3.0 μm; minimum stubby spine size is 10 voxels; minimum size for non-stubby spines is five voxels; spine classifiers for neck ratio (1.1) and thin spine ratio (2.5). Spines on all branches of a dendrite were calculated within Sholl's circles at 1 μm increments in radii, relative to the cell body. Data are plotted at 10 μm increments.

### Statistical analysis

Data are presented as means ± standard error. Two-tailed unpaired Student's *t*-test was used for analyzing morphology and spine density between control and *Tubb5* shRNA treatment. One-way ANOVA with Bonferroni *post hoc* test was used for comparing the data between controls and overexpression of

wild-type TUBB5 and its variants M299V, V353I and E401K. ANCOVA was performed in order to assess the slope and elevation of the curves generated from Sholl analysis (41). *, **, *** and **** indicated $P < 0.05$, $P < 0.01$, $P < 0.001$ and $P < 0.0001$, respectively. A $P$-value of $<0.05$ was considered statistically significant. Two-way ANOVA with Bonferroni's *post hoc* test was used to assess dendritic spine densities and distribution of spine shapes (stubby, thin and mushroom). All statistical data generated in this study are provided in Supplementary Material, Table S3.

### Live cell imaging and analysis of EB3 comets in neural cells

Neuro-2a cells were seeded in 3 cm dishes designed for live cell imaging. On the day of transfection, Lipofectamine (Life Technologies, USA) was mixed with a pSuper vector containing either scramble or *Tubb5* shRNA together with GFP-EB3 expression construct; or with a pCIG vector encoding FLAG-tagged versions of wild-type TUBB5 (or missense variants) together with GFP-EB3 construct. The ratio of EB3-GFP vector to shRNA vector (or *TUBB5* vector) was 0.5:1, and cells were imaged 48 h posttransfection. Prior to imaging, cells were allowed to adapt for at least 30 min at 37°C within the chamber. EB3 comet tracking was performed with a Leica SP5 microscope; time lapse images of comets were recorded at 1 s intervals, for a total of 2 min. Scans were performed at three $z$-positions at 0.3 μm spacing. Stacks were analyzed using ImarisTrack 7.6 (Bitplane), and average speeds of tracked comets were calculated between each time point.

## AUTHOR CONTRIBUTIONS

J.I.H. and D.A.K. conceived the project, whereas L.N., M.A.H., Z.Q., S.S.L. and M.B. performed *in utero* electroporation and cell culture experiments; and J.Z., K.S.L.T. together with J.M.G. performed live imaging of cultured cells. L.N., M.A.H. and J.I.H. analyzed data with M.H. J.I.H. and L.N. wrote the manuscript with D.A.K. All authors commented on the manuscript.

## SUPPLEMENTARY MATERIAL

Supplementary Material is available at *HMG* online.

*Conflict of Interest statement*. None declared.

## FUNDING

The Australian Regenerative Medicine Institute is supported by grants from the State Government of Victoria and the Australian Government. D.A.K. acknowledges the generous support of Boehringer Ingelheim and the following FWF grants (P24367, P21092 and I914). J.I.H. is supported by an NH&MRC Career Development Fellowship (ID:1011505), as well as a Monash Senior Research Fellowship.

## REFERENCES

1. Ayala, R., Shu, T. and Tsai, L.H. (2007) Trekking across the brain: the journey of neuronal migration. *Cell*, **128**, 29–43.
2. Heng, J.I., Chariot, A. and Nguyen, L. (2010) Molecular layers underlying cytoskeletal remodelling during cortical development. *Trends Neurosci.*, **33**, 38–47.
3. LoTurco, J.J. and Bai, J. (2006) The multipolar stage and disruptions in neuronal migration. *Trends Neurosci.*, **29**, 407–413.
4. Parnavelas, J.G., Alifragis, P. and Nadarajah, B. (2002) The origin and migration of cortical neurons. *Prog. Brain Res.*, **136**, 73–80.
5. Barnes, A.P. and Polleux, F. (2009) Establishment of axon-dendrite polarity in developing neurons. *Annu. Rev. Neurosci*., **32**, 347–381.
6. Whitford, K.L., Dijkhuizen, P., Polleux, F. and Ghosh, A. (2002) Molecular control of cortical dendrite development. *Annu. Rev. Neurosci.*, **25**, 127–149.
7. Vallee, R.B., Seale, G.E. and Tsai, J.W. (2009) Emerging roles for myosin II and cytoplasmic dynein in migrating neurons and growth cones. *Trends Cell. Biol.*, **19**, 347–355.
8. Tischfield, M.A. and Engle, E.C. (2010) Distinct alpha- and beta-tubulin isotypes are required for the positioning, differentiation and survival of neurons: new support for the 'multi-tubulin' hypothesis. *Biosci. Rep.*, **30**, 319–330.
9. Cushion, T.D., Dobyns, W.B., Mullins, J.G., Stoodley, N., Chung, S.K., Fry, A.E., Hehr, U., Gunny, R., Aylsworth, A.S., Prabhakar, P. *et al.* (2013) Overlapping cortical malformations and mutations in TUBB2B and TUBA1A. *Brain*, **136**, 536–548.
10. Jaglin, X.H., Poirier, K., Saillour, Y., Buhler, E., Tian, G., Bahi-Buisson, N., Fallet-Bianco, C., Phan-Dinh-Tuy, F., Kong, X.P., Bomont, P. *et al.* (2009) Mutations in the beta-tubulin gene TUBB2B result in asymmetrical polymicrogyria. *Nat. Genet.*, **41**, 746–752.
11. Keays, D.A., Tian, G., Poirier, K., Huang, G.J., Siebold, C., Cleak, J., Oliver, P.L., Fray, M., Harvey, R.J., Molnar, Z. *et al.* (2007) Mutations in alpha-tubulin cause abnormal neuronal migration in mice and lissencephaly in humans. *Cell*, **128**, 45–57.
12. Poirier, K., Saillour, Y., Bahi-Buisson, N., Jaglin, X.H., Fallet-Bianco, C., Nabbout, R., Castelnau-Ptakhine, L., Roubertie, A., Attie-Bitach, T., Desguerre, I. *et al.* (2010) Mutations in the neuronal ss-tubulin subunit TUBB3 result in malformation of cortical development and neuronal migration defects. *Hum. Mol. Genet.*, **19**, 4462–4473.
13. Tischfield, M.A., Baris, H.N., Wu, C., Rudolph, G., Van Maldergem, L., He, W., Chan, W.M., Andrews, C., Demer, J.L., Robertson, R.L. *et al.* (2010) Human TUBB3 mutations perturb microtubule dynamics, kinesin interactions, and axon guidance. *Cell*, **140**, 74–87.
14. Cushion, T.D., Paciorkowski, A.R., Pilz, D.T., Mullins, J.G., Seltzer, L.E., Marion, R.W., Tuttle, E., Ghoneim, D., Christian, S.L., Chung, S.K. *et al.* (2014) De novo mutations in the beta-tubulin gene TUBB2A cause simplified gyral patterning and infantile-onset epilepsy. *Am. J. Hum. Genet.*, **94**, 634–641.
15. Poirier, K., Keays, D.A., Francis, F., Saillour, Y., Bahi, N., Manouvrier, S., Fallet-Bianco, C., Pasquier, L., Toutain, A., Tuy, F.P. *et al.* (2007) Large spectrum of lissencephaly and pachygyria phenotypes resulting from de novo missense mutations in tubulin alpha 1A (TUBA1A). *Hum. Mutat.*, **28**, 1055–1064.
16. Saillour, Y., Broix, L., Bruel-Jungerman, E., Lebrun, N., Muraca, G., Rucci, J., Poirier, K., Belvindrah, R., Francis, F. and Chelly, J. (2013) Beta tubulin isoforms are not interchangeable for rescuing impaired radial migration due to Tubb3 knockdown. *Hum. Mol. Genet*., **23**, 1516–1526.
17. Breuss, M., Heng, J.I., Poirier, K., Tian, G., Jaglin, X.H., Qu, Z., Braun, A., Gstrein, T., Ngo, L., Haas, M. *et al.* (2012) Mutations in the beta-tubulin gene TUBB5 cause microcephaly with structural brain abnormalities. *Cell Rep.*, **2**, 1554–1562.
18. Noctor, S.C., Martinez-Cerdeno, V., Ivic, L. and Kriegstein, A.R. (2004) Cortical neurons arise in symmetric and asymmetric division zones and migrate through specific phases. *Nat. Neurosci.*, **7**, 136–144.
19. Hand, R., Bortone, D., Mattar, P., Nguyen, L., Heng, J.I., Guerrier, S., Boutt, E., Peters, E., Barnes, A.P., Parras, C. *et al.* (2005) Phosphorylation of Neurogenin2 specifies the migration properties and the dendritic morphology of pyramidal neurons in the neocortex. *Neuron*, **48**, 45–62.
20. Gutierrez, H., Dolcet, X., Tolcos, M. and Davies, A. (2004) HGF regulates the development of cortical pyramidal dendrites. *Development*, **131**, 3717–3726.

21. Horch, H.W. and Katz, L.C. (2002) BDNF release from single cells elicits local dendritic growth in nearby neurons. *Nat. Neurosci.*, **5**, 1177–1184.
22. Hering, H. and Sheng, M. (2001) Dendritic spines: structure, dynamics and regulation. *Nat. Rev. Neurosci.*, **2**, 880–888.
23. Stepanova, T., Slemmer, J., Hoogenraad, C.C., Lansbergen, G., Dortland, B., De Zeeuw, C.I., Grosveld, F., van Cappellen, G., Akhmanova, A. and Galjart, N. (2003) Visualization of microtubule growth in cultured neurons via the use of EB3-GFP (end-binding protein 3-green fluorescent protein). *J. Neurosci.*, **23**, 2655–2664.
24. Tian, G., Jaglin, X.H., Keays, D.A., Francis, F., Chelly, J. and Cowan, N.J. (2010) Disease-associated mutations in TUBA1A result in a spectrum of defects in the tubulin folding and heterodimer assembly pathway. *Hum. Mol. Genet.*, **19**, 3599–3613.
25. Kriegstein, A.R. and Noctor, S.C. (2004) Patterns of neuronal migration in the embryonic cortex. *Trends Neurosci.*, **27**, 392–399.
26. Baraban, M., Anselme, I., Schneider-Maunoury, S. and Giudicelli, F. (2013) Zebrafish embryonic neurons transport messenger RNA to axons and growth cones in vivo. *J. Neurosci.*, **33**, 15726–15734.
27. Niblock, M.M., Brunso-Bechtold, J.K. and Riddle, D.R. (2000) Insulin-like growth factor I stimulates dendritic growth in primary somatosensory cortex. *J. Neurosci.*, **20**, 4165–4176.
28. Cossart, R., Dinocourt, C., Hirsch, J.C., Merchan-Perez, A., De Felipe, J., Ben-Ari, Y., Esclapez, M. and Bernard, C. (2001) Dendritic but not somatic GABAergic inhibition is decreased in experimental epilepsy. *Nat. Neurosci.*, **4**, 52–62.
29. Goldberg, E.M. and Coulter, D.A. (2013) Mechanisms of epileptogenesis: a convergence on neural circuit dysfunction. *Nat. Rev. Neurosci.*, **14**, 337–349.
30. Gu, J., Firestein, B.L. and Zheng, J.Q. (2008) Microtubules in dendritic spine development. *J. Neurosci.*, **28**, 12120–12124.
31. Hu, X., Viesselmann, C., Nam, S., Merriam, E. and Dent, E.W. (2008) Activity-dependent dynamic microtubule invasion of dendritic spines. *J. Neurosci.*, **28**, 13094–13105.
32. Jaworski, J., Kapitein, L.C., Gouveia, S.M., Dortland, B.R., Wulf, P.S., Grigoriev, I., Camera, P., Spangler, S.A., Di Stefano, P., Demmers, J. *et al.* (2009) Dynamic microtubules regulate dendritic spine morphology and synaptic plasticity. *Neuron*, **61**, 85–100.
33. Bradke, F. and Dotti, C.G. (1999) The role of local actin instability in axon formation. *Science*, **283**, 1931–1934.
34. Witte, H., Neukirchen, D. and Bradke, F. (2008) Microtubule stabilization specifies initial neuronal polarization. *J. Cell. Biol.*, **180**, 619–632.
35. Francis, F., Koulakoff, A., Boucher, D., Chafey, P., Schaar, B., Vinet, M.C., Friocourt, G., McDonnell, N., Reiner, O., Kahn, A. *et al.* (1999) Doublecortin is a developmentally regulated, microtubule-associated protein expressed in migrating and differentiating neurons. *Neuron*, **23**, 247–256.
36. Gleeson, J.G., Lin, P.T., Flanagan, L.A. and Walsh, C.A. (1999) Doublecortin is a microtubule-associated protein and is expressed widely by migrating neurons. *Neuron*, **23**, 257–271.
37. Horesh, D., Sapir, T., Francis, F., Wolf, S.G., Caspi, M., Elbaum, M., Chelly, J. and Reiner, O. (1999) Doublecortin, a stabilizer of microtubules. *Hum. Mol. Genet.*, **8**, 1599–1610.
38. Neale, B.M., Kou, Y., Liu, L., Ma'ayan, A., Samocha, K.E., Sabo, A., Lin, C.F., Stevens, C., Wang, L.S., Makarov, V. *et al.* (2012) Patterns and rates of exonic de novo mutations in autism spectrum disorders. *Nature*, **485**, 242–245.
39. Pinto, D., Pagnamenta, A.T., Klei, L., Anney, R., Merico, D., Regan, R., Conroy, J., Magalhaes, T.R., Correia, C., Abrahams, B.S. *et al.* (2010) Functional impact of global rare copy number variation in autism spectrum disorders. *Nature*, **466**, 368–372.
40. Heng, J.I., Nguyen, L., Castro, D.S., Zimmer, C., Wildner, H., Armant, O., Skowronska-Krawczyk, D., Bedogni, F., Matter, J.M., Hevner, R. *et al.* (2008) Neurogenin 2 controls cortical neuron migration through regulation of Rnd2. *Nature*, **455**, 114–118.
41. Hammond, V.E., Gunnersen, J.M., Goh, C.P., Low, L.H., Hyakumura, T., Tang, M.M., Britto, J.M., Putz, U., Howitt, J.A. and Tan, S.S. (2013) Ndfip1 Is Required for the Development of Pyramidal Neuron Dendrites and Spines in the Neocortex. *Cereb. Cortex*. doi: 10.1093/cercor/bht191.